SIAM J. CONTROL OPTIM.
Vol. 48, No. 1, pp. 351–372

NONUNIFORM COVERAGE AND CARTOGRAMS*

FRANCOIS LEKIEN† AND NAOMI EHRICH LEONARD‡

Abstract. In this paper, we investigate nonuniform coverage of a planar region by a network of autonomous, mobile agents. We derive centralized nonuniform coverage control laws from uniform coverage algorithms using cartograms, transformations that map nonuniform metrics to a near Euclidean metric. We also investigate time-varying coverage metrics and the design of control algorithms to cover regions with slowly varying, nonuniform metrics. Our results are applicable to the design of mobile sensor networks, notably when the coverage metric varies as data is collected such as in the case of an information metric. The results apply also to the study of animal groups foraging for food that is nonuniformly distributed and possibly changing.

Key words. cartogram, optimal coverage, mobile sensor networks, adaptive sampling

AMS subject classifications. 49K99, 65J10, 35G10

DOI. 10.1137/070681120

1. Introduction.

Sensor networks in space, in the air, on land, and in the ocean provide the opportunity for unprecedented observational capability. An important problem in this context is to determine how best to distribute sensors over a given area in which the observational field is distributed so that the likelihood of detecting an event of interest is maximized. If the probability distribution of the event is uniform over the area, then the optimal solution is uniform coverage, i.e., uniform distribution of sensors. On the other hand, if this probability distribution is nonuniform, then the sensors should be more (less) densely distributed in subregions with higher (lower) event probability. Further, if the probability distribution changes with time, then the nonuniform distribution should likewise change with time.

A related coverage problem derives from the classic objective analysis (OA) mapping error in problems of sampling (possibly time-varying) scalar fields, e.g., temperature in the ocean [3]. OA is linear statistical estimation based on specified field statistics, and the mapping error provides a measure of statistical uncertainty of the model as a function of where and when the data is taken. Since reduced uncertainty, equivalent to increased entropic information, implies better measurement coverage, OA mapping error can be used as a coverage metric [3, 15]. If the a priori error correlation between any two points in the plane is homogeneous and isotropic, then uniform coverage will be optimal initially. However, the optimal coverage solution will not be static (unless the scalar field of interest changes very quickly), since, once a particular location has been sampled, it should not be sampled again until the measurement value has decayed sufficiently.

Robotic vehicles carrying sensors in space, in the air, on land, and in the ocean make possible mobile sensor networks that can adapt to changing coverage requirements. Given a coverage metric that is independent of time and of the history of

*Received by the editors January 26, 2007; accepted for publication (in revised form) August 10, 2008; published electronically February 11, 2009. This research was supported by the Jules Reyers Foundation and ONR grants N00014-02-1-0826 and N00014-04-1-0534.

http://www.siam.org/journals/sicon/48-1/68112.html

†École Polytechnique CP 165/11, Université Libre de Bruxelles, B-1050 Brussels, Belgium (lekien@ulb.ac.be).

‡Department of Mechanical and Aerospace Engineering, Princeton University, Princeton, NJ 08544 (naomi@princeton.edu).

samples taken, the goal is to design coordinated control dynamics for the vehicles that yield convergence to the maximum coverage configuration from arbitrary initial conditions. A second objective is to extend these coordinated control dynamics to the case in which the coverage metric definition changes in time or, as in the case of the OA error metric, as a function of past measurement locations and times.

Coverage problems have a compelling analogy in possible models of social foraging by animal groups. Backed by observations of animal behavior across a number of species, biologists model distribution of animals over patchy resource environments according to a measure of patch suitability that depends on factors such as resource richness or conditions for survival [7, 2, 20]. Suitability varies with animal density; a typical assumption is that suitability decreases with increasing animal population. For example, suitability declines when more animals converge on a given patch since resources (e.g., prey) may be limited, and thus average consumption rates go down with more hungry consumers. Since animals prefer patches with higher suitability, nonuniformity in the distribution of resources (i.e., the suitability) reflects nonuniformity in the distribution of the animal group. As in the case of the OA mapping error metric that changes as samples are taken, suitability decreases in time as animals consume (and animals will abandon patches where suitability has declined). By this analogy, coverage studies of changing, nonuniform environments may prove useful in helping to explain how animal groups move and redistribute.

Several contributions have been made to the design of coverage algorithms for a group of dynamic agents, including [4, 18, 17, 5] and the references therein. In [4], uniform coverage algorithms are derived using Voronoi cells and gradient laws for distributed dynamical systems. Uniform constrained coverage control is addressed in [18], where the constraint is a minimum limit on node degree. Node degree refers to the number of neighbors for each agent, where a neighbor is any other agent that is sufficiently close by. Virtual potentials enable repulsion between agents to maximize coverage and attraction between agents to enforce the constraint. In [17], gradient control laws are proposed to move sensors to a configuration that maximizes expected event detection frequency. Local rules are enforced by defining a sensing radius for each agent, which also makes computations simpler. The approach is demonstrated for a nonuniform but symmetric density field with and without communication constraints. Further results for distributed coverage control are presented in [5] for a coverage metric defined in terms of the Euclidean metric with a weighting factor that allows for nonuniformity. As in [4], the methodology makes use of Voronoi cells and Lloyd descent algorithms.

In this paper we concentrate exclusively on two-dimensional planar regions, and we propose an approach to coverage control that makes use of existing algorithms designed for uniform coverage and extends these to nonuniform metrics. We are particularly interested in metrics defined in terms of non-Euclidean distance functions that effectively stretch and shrink space in lower and higher density regions of a given space. This yields optimal configurations where the resource or information is evenly distributed among the agents. Non-Euclidean distance metrics present challenges to existing techniques. For example, in the case of [4, 5], computing Voronoi cells with non-Euclidean metrics is computationally complex. For each point on a dense grid, one needs to compute the (non-Euclidean) distance to each agent and find the minimum. Computing Voronoi cells for a non-Euclidean metric is therefore much more demanding than the corresponding problem with an Euclidean metric where the polygonal boundaries of the Voronoi cells can be computed directly.

The first step in our method is to compute a nonuniform change of coordinates

on the original compact set with a non-Euclidean metric that maps to a new compact set with a near Euclidean metric. Such a map is called a *cartogram*. Inspired by the work of Gastner and Newman [9], we compute the cartogram from a diffusion equation. Gastner and Newman used cartograms in several applications, including the representation of election results [11] and the optimal design of spatial distribution networks [10]. For these problems, it is sufficient to compute single cartograms, while we are interested in computing a series of cartograms for feedback control. Accordingly, we propose a method to compute cartograms that vary smoothly as a function of the density distribution.

A uniform control law can be used in the cartogram space since the metric in this space is almost Euclidean. The preimage of the control law yields convergent dynamics in the original space. We prove under certain conditions that these convergent dynamics optimize the nonuniform coverage metric. We show how to extend the approach to the case of a time-varying metric.

A limitation of our approach is the centralized computation of the cartogram. However, we note that the density function does not need to be known a priori; it can be measured or computed by the agents in real time. For example, the changing OA metric can be computed only on the fly since it is a function of where and when samples have been taken.

In section 2 we review, as an example, the uniform coverage control of [4]. We describe the nonuniform coverage problem in section 3. Cartograms are defined in section 4. Gastner and Newman's method for computing cartograms using the diffusion equation is reviewed, and our new approach to computing smooth cartograms is presented. In section 5 we describe and prove our approach to nonuniform coverage control that makes use of cartograms. Section 6 provides error estimates for the examples studied, and the case of time-varying metrics is addressed in section 7. Conclusions and future directions are given in section 8.

2. Uniform coverage. A number of different metrics and different coordinated control strategies have been developed for uniform coverage, as described above. In this section, as a motivating and useful example, we review the uniform coverage approach and result of Cortés and Bullo, who devised a robust and efficient control scheme to optimize the configuration of a group of robotic vehicles carrying sensors [4]. They consider a group of n vehicles moving in a region $\mathcal{D}$, with a polygonal boundary $\partial\mathcal{D}$. The vehicles obey first-order dynamics:

$$\dot{\mathbf{x}}_i = \mathbf{u}_i(\mathbf{x}_1, \ldots, \mathbf{x}_n), \tag{2.1}$$

where $\mathbf{x}_i$ is the position of the ith vehicle and $\mathbf{u}_i$ is the control input to the ith vehicle.

The goal is to bring the robots, from their initial positions, to a (static) configuration that maximizes coverage of the domain. To define *maximum coverage*, Cortés and Bullo consider multicenter metric functions such as

$$\Phi(\mathbf{x}_1, \mathbf{x}_2, \ldots, \mathbf{x}_n) = \max_{\mathbf{x}\in\mathcal{D}} \Big\{ \min_{i=1\cdots n} d(\mathbf{x}, \mathbf{x}_i) \Big\}, \tag{2.2}$$

where $d(\mathbf{x}, \mathbf{x}_i) = \|\mathbf{x} - \mathbf{x}_i\|$ is the Euclidean distance. Given the position of the n vehicles, computing the metric requires computing the distance from any point $\mathbf{x} \in \mathcal{D}$ to the closest vehicle. The metric Φ is equal to the largest of these distances. As a result, the maximum distance between any point of the domain and the closest vehicle is always smaller than or equal to Φ. Intuitively, a smaller Φ implies that the corresponding array of vehicles $\mathbf{x}_i$ achieves a better coverage of the domain $\mathcal{D}$.

Assuming that all of the vehicles have the same constant speed, Φ is proportional to the maximum time it takes for a vehicle to reach an arbitrary point of the domain. For this reason, Cortés and Bullo define optimal coverage as the minimum of the cost function Φ.

One of the main results of [4] is the development of a stable procedure to bring the vehicles into a configuration that minimizes the metric Φ. To this end, the Voronoi cell of each vehicle is computed repeatedly. The Voronoi cell for the ith vehicle is a polygonal subset of the domain $\mathcal{D}$ that contains all of the points that are closer to the ith vehicle than any other vehicle. Each vehicle is then directed to move toward the circumcenter of its Voronoi cell (see Figure 1). Once all the vehicles reach the circumcenter of their Voronoi cell, the coverage metric Φ is minimum (see the last panel of Figure 1). Cortés and Bullo show that, from any initial position where the vehicles are not exactly on top of each other, their algorithm converges toward the optimal configuration.

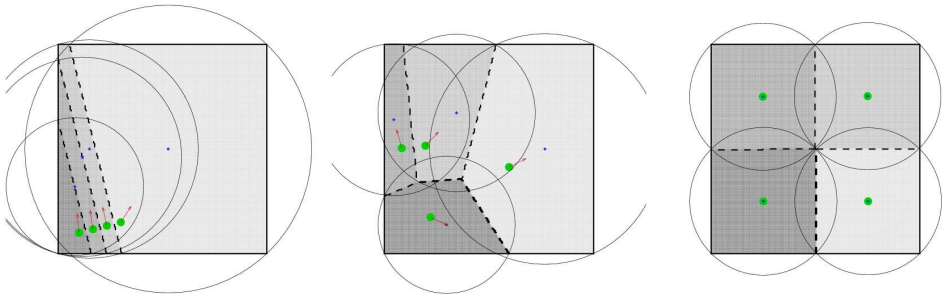

FIG. 1. *Convergence to static uniform coverage.* Thick dots: *Position of the four agents.* Shaded polygons: *Voronoi cell for each agent.* Large circles: *Circumcircle of each Voronoi cell.* Diamonds: *Centers of each circumcircle (i.e., circumcenters).* Arrows: *Velocity of the vehicles (oriented along the segment joining the agents to the circumcenter of their Voronoi cell).*

3. Nonuniform coverage. In the present paper we develop an approach that extends optimal coverage strategies to more general metrics, notably to nonuniform and time-varying metrics. Nonuniform metrics are motivated by coverage problems in environments with nonuniformly distributed information or resources. The objective is to produce distributions of agents that match the inhomogeneities in the information or resource field. We are particularly interested in metrics defined in terms of a (possibly time-varying) distance function that is non-Euclidean. A non-Euclidean distance function stretches high density areas and shrinks low density areas. With a coverage metric that depends on such a distance function, individual agents can be organized so that information or resources are equally distributed among them. In other words, each agent has a "dominance region" (e.g., Voronoi cell) and, irrespective of the size of these regions, we want the amount of information or the resource to be equal in each agent's cell.

Notice that this objective is slightly different from the approach of Cortés and Bullo. In [4], the region of dominance of an agent is flexible and might include points that can be reached more easily by other agents. In this paper, we consider the dominance region of an agent $\mathbf{x}_i$ as a defined region containing all of the points that are closer to $\mathbf{x}_i$ than any other agent in the sense of the non-Euclidean metric, i.e., that can be reached more easily by agent $\mathbf{x}_i$ than by any other agent, where ease in

reaching a point depends on density. In other words, the dominance region is still a Voronoi cell, and the nonuniform density is introduced through the distance function used to compute the Voronoi cells. The nonuniform distance shrinks along paths where resources are sparse and increases along paths where resources are plentiful.

Recall that the Euclidean distance between two points is also the length of the shortest path between the two points, or

$$\|\mathbf{x} - \mathbf{x}_i\| = \min_{\mathcal{C}_{\mathbf{x}}^{\mathbf{x}_i}} \left\{ \int_{\mathcal{C}_{\mathbf{x}}^{\mathbf{x}_i}} \mathrm{dl} \right\},$$

where $\mathcal{C}_{\mathbf{x}}^{\mathbf{x}_i}$ is an arbitrary path from $\mathbf{x}$ to $\mathbf{x}_i$. If the density of information $\rho : \mathcal{D} \to \mathbb{R}_0^+$ is not uniform, then we can define a non-Euclidean distance:

$$d_\rho(\mathbf{x}, \mathbf{x}_i) = \min_{\mathcal{C}_{\mathbf{x}}^{\mathbf{x}_i}} \left\{ \int_{\mathcal{C}_{\mathbf{x}}^{\mathbf{x}_i}} \sqrt{\rho}\, \mathrm{dl} \right\}.$$

The distance between two points in a low-density area is less than the Euclidean distance. The shortest path between two points might be curved in order to avoid peaks of ρ. High density implies that the distances are stretched; hence more vehicles are needed in the area. The region of dominance of each agent is still its Voronoi cell, but the nonuniform distance changes the shape of the cell. As an example see the bottom right panel of Figure 6, which shows four vehicles distributed optimally with respect to a non-Euclidean metric; in this example, the peak density is in the lower right corner of the region.

Note that we use the square root of the function ρ and not the function ρ itself to weight the distance integral. The reason for this choice is the fact that, in two dimensions, multiplying the distances in each direction by $\sqrt{\rho}$ implies a net volume (or density) change of ρ. It is also worth noting that weighting the distance integral by a negative function is not acceptable, as some distances would become negative.

In this paper we assume that the coverage metric Φ is a functional of a distance function d_ρ, which depends on the positions of the agents $\mathbf{x}_i$ and the domain $\mathcal{D}$, denoted

$$\Phi = (\Phi[d_\rho])\,(\mathbf{x}_i, \ldots, \mathbf{x}_n; \mathcal{D}). \tag{3.1}$$

Clearly, one can use any metric Φ that involves only the Euclidean distance, such as the multicenter function (2.2), and make it inhomogeneous by replacing the Euclidean distance d with the weighted distance d_ρ. If ρ represents the density distribution for information or resources, then optimal coverage solutions correspond to evenly distributed information or resources to each agent's "dominance region."

In [5], Cortés et al. design coverage control algorithms for a density-dependent metric defined, as a function of a given array of agents $\mathbf{x}_1, \mathbf{x}_2, \ldots, \mathbf{x}_n$, by

$$\Phi(\mathbf{x}_1, \mathbf{x}_2, \ldots, \mathbf{x}_n) = \int_{\mathcal{D}} \min_i \Big\{ f(d(\mathbf{x}, \mathbf{x}_i))\, \rho(\mathbf{x}) \Big\}\, \mathrm{d}\mathbf{x},$$

where f is a nondecreasing function and ρ is the distribution density function. Because the metric depends on the Euclidean distance function, the cost function can be rewritten as

$$\Phi(\mathbf{x}_1, \mathbf{x}_2, \ldots, \mathbf{x}_n) = \sum_{i=1}^{n} \int_{V_i} f(d(\mathbf{x}, \mathbf{x}_i))\, \rho(\mathbf{x})\, \mathrm{d}\mathbf{x},$$

where the Voronoi cells V_i are defined also by the Euclidean distance function as

$$V_i = \left\{ \mathbf{x} \in \mathcal{D} \;\middle|\; d(\mathbf{x}, \mathbf{x}_i) \leq d(\mathbf{x}, \mathbf{x}_j) \;\forall j \neq i \right\}.$$

As shown in [5], this means that the cost function can be seen as the contribution of n dominance regions V_i, each of which is the Voronoi cell of an agent. Although this metric yields coverage solutions that are nonuniform, the information or resource will nonetheless *not* be equally distributed among corresponding dominance regions.

In this paper, we are interested in cost functions of the form (3.1). Indeed, a metric based on a nonuniform distance d_ρ is more closely related to information gathering and sensing array optimization.

One such problem is the detection of acoustic signals. In this case, $\sqrt{\rho}$ represents the nonuniform refractive index of the environment. The objective is to place the sensors in such a way that they can detect sources anywhere. In other words, one needs to minimize the weighted distance d_ρ between any point in the domain and the agents.

Another typical problem consists in increasing the ability of the array on an uneven terrain. This situation is typical for mine hunting arrays in a standby mode; the optimal configuration minimizes the time that it would take to send one of the agents to a newly detected mine. In this case, the square root of $\rho(\mathbf{x})$ represents the roughness of the terrain, the infinitesimal time it takes to cross an infinitesimal path located in $\mathbf{x}$. The goal is to position the agents in such a way that any point of the domain can be reached by one of the agents in minimum time. The optimal solution corresponds to the minimum of the cost function in (3.1), where $d_\rho(\mathbf{x}, \mathbf{y})$ is the minimum travel time between points $\mathbf{x}$ and $\mathbf{y}$.

A variant of the algorithm of [4, 5] could be used to optimize the coverage with a nonuniform metric defined in terms of a non-Euclidean distance function. Indeed, one can define Voronoi cells based on the non-Euclidean distance function. The boundaries of such Voronoi cells are, however, not polygonal, and their computation is complex and time-consuming. To compute the distance between two points $\mathbf{a}$ and $\mathbf{b}$, one needs to consider any path between $\mathbf{a}$ and $\mathbf{b}$ and to find the minimum of $\int_{\mathcal{C}_\mathbf{a}^\mathbf{b}} \sqrt{\rho}\, \mathrm{d}l$. Our approach, which involves computing cartograms, is, as will be illustrated below, a much simpler and faster operation.

In this paper, we assume that a particular cost function of the form (3.1) has been selected and that there exists a stable algorithm that brings a group of vehicles to the minimum of Φ for the Euclidean distance. We provide a methodology to modify this algorithm when the non-Euclidean distance (e.g., terrain roughness, acoustic refraction) is used.

4. Cartograms. Our approach to deriving coverage control strategies for nonuniform and time-varying metrics is to find a standard method to modify a control law defined for the Euclidean metric in such a way that it remains stable and converges to the minimum of the nonuniform metric.

The method that we develop is based on a nonuniform change of coordinates that transforms the domain $\mathcal{D}$ with the non-Euclidean distance into another compact set $\mathcal{D}'$ where the distance is Euclidean or near Euclidean. Such transformations are commonly referred to as "cartograms" in computer graphics.

To motivate the notion of cartogram, consider how poorly census and election results are represented using standard geographical projections; such data are better plotted on maps in which the sizes of geographic regions such as countries or provinces

appear in proportion to their population (as opposed to the geographical area). Such maps, which are cartograms, transform the physical space $\mathcal{D}$ into a fictitious space $\mathcal{D}'$ where the area element A is proportional to a nonuniform density $\rho : \mathcal{D} \to \mathbb{R}_0^+$.

DEFINITION 4.1 (cartogram). *Given a compact domain $\mathcal{D} \subset \mathbb{R}^2$ and a density function $\rho : \mathcal{D} \to \mathbb{R}_0^+$, a cartogram is a C^1 (continuous everywhere and with continuous derivatives almost everywhere) mapping $\phi : \mathcal{D} \to \mathcal{D}' : \mathbf{x} \to \phi(\mathbf{x})$ such that*

$$\det\left(\frac{\partial \phi}{\partial \mathbf{x}}\right) = \rho.$$

It is standard in the literature to define a cartogram as a change of coordinates as above but such that $\det\big(\frac{\partial \phi}{\partial \mathbf{x}}(\mathbf{x})\big) = k\rho(\mathbf{x}) > 0$; i.e., the transformation multiplies the area element by the density function ρ and an arbitrary constant $k > 0$. Without loss of generality, we assume that $k = 1$. If that is not the case, then one can multiply ϕ by k^{-1}.

As an example, Figure 2 shows the linguistic distribution in Belgium. The left panel of Figure 2 shows the five Flemish-speaking provinces and the five French-speaking provinces on an equal-area projection (Belgian conic conformal Lambert projection). The center panel gives the level sets of the population density and reveals that, while geographically smaller than its French counterpart, the Flemish region is much more densely populated and accounts for the majority of the country's population.

The right panel of Figure 2 is the cartogram of the country based on population density. In this projection, areas are proportional to the density of population. Such a cartogram is more adequate for plotting census and election results since the national outcome of the election or referendum is based on the principle of "one vote per citizen" and not "one vote per unit of area." Our method for computing cartograms, inspired by the approach of Gastner and Newman [9], is presented in this section.

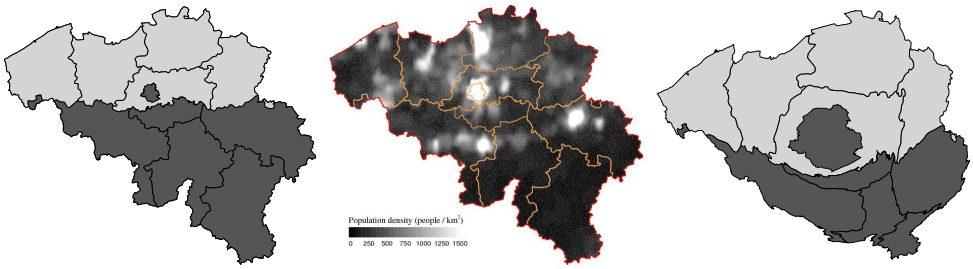

FIG. 2. *Linguistic distribution and population density in Belgium.* Left panel: *Equal-area (Belgian Lambert) projection. Light gray represents Flemish provinces. Dark gray stands for French-speaking provinces and the Brussels-Capital area.* Center panel: *Density of population binned on* 5km × 5km *cells (source: Columbia University's Center for International Earth Science Information Network).* Right panel: *Cartogram of the country based on population density. Areas in this projection are proportional to population density and correctly depict the linguistic distribution.*

Given a domain $\mathcal{D}$ and a density function ρ, there are infinitely many possible cartograms. As stated in [9], the objective is to minimize the distortion of the original figure. A perfect cartogram would not introduce any deformation and would satisfy

$$\frac{\partial \phi}{\partial \mathbf{x}} = \sqrt{\rho}\, \mathbb{I},$$

where $\mathbb{I}$ is the identity matrix. Clearly, such a cartogram does not exist for most density functions ρ. Nevertheless, we seek to reduce the distortion and to minimize $\left\| \frac{\partial \phi}{\partial \mathbf{x}} - \sqrt{\rho}\,\mathbb{I} \right\|$, where $\|\cdot\|$ is any norm on the space of 2×2 matrices. Accordingly, we make the following definitions.

DEFINITION 4.2 (perfect cartogram). *For a given density function ρ, a perfect cartogram, if it exists, is a cartogram such that $\left\| \frac{\partial \phi}{\partial \mathbf{x}} - \sqrt{\rho}\,\mathbb{I} \right\| = 0$.*

DEFINITION 4.3 (ideal cartogram). *For a given density function ρ, an ideal cartogram is given by*

$$\operatorname*{Argmin}_{\phi} \left\| \frac{\partial \phi}{\partial \mathbf{x}} - \sqrt{\rho}\,\mathbb{I} \right\| .$$

4.1. Cartograms with fixed boundaries. Recently, Gastner and Newman [9] showed how to construct a cartogram using a diffusion equation. Although perfect cartograms usually do not exist and there is no guarantee that a cartogram obtained using diffusion is an ideal cartogram, the work of Gastner and Newman has shown that, among all known methods to compute cartograms, the diffusion method introduces very little distortion and produces maps that are the closest to the perfect diagonal form $\sqrt{\rho}\,\mathbb{I}$.

To describe the method of [9], we first address the case in which, for a given ρ, the normal component of $\nabla\rho$ along the boundary $\partial\mathcal{D}$ vanishes. In this case, there exists a cartogram $\phi : \mathcal{D} \to \mathcal{D}'$, where $\mathcal{D}' = \mathcal{D}$. To show the existence of the cartogram and to determine a method to compute it, we imagine that the domain $\mathcal{D}$ is filled with a fluid whose initial density is given by ρ. As time evolves, the gradient of the density creates motion and the density of the fluid tends to homogenize. Let us consider the density $c(\mathbf{x}, t)$ at point $\mathbf{x}$ and time t. It satisfies the diffusion equation

$$\frac{\partial c}{\partial t} = \nu \Delta c \,,$$

where the initial condition is $c(\mathbf{x}, 0) = \rho(\mathbf{x})$, the boundary condition is $\frac{\partial c}{\partial n} = 0$, and $\nu > 0$ is arbitrary. For $t \to +\infty$, the density c tends to a constant distribution c_∞ and, at any time t and at any position $\mathbf{x}$, we have $c(\mathbf{x}, t) > 0$. As a result, we can define a velocity field:

$$\mathbf{v}(\mathbf{x}, t) = -\nu \, \frac{\nabla c}{c}(\mathbf{x}, t).$$

Given the initial position $\mathbf{x}_0$ at which a particle is released at time $t = 0$, the velocity field above determines the position at any later time t. The flow (i.e., the trajectories) of the velocity field is a function of time and of the initial position. We denote by $\mathbf{x}(t; \mathbf{x}_0)$ the unique trajectory that satisfies

$$\begin{cases} \dot{\mathbf{x}} = \mathbf{v}\left(\mathbf{x}(t; \mathbf{x}_0), t\right), \\ \mathbf{x}(0; \mathbf{x}_0) = \mathbf{x}_0. \end{cases}$$

The domain $\mathcal{D}$ is compact; hence the trajectories $\mathbf{x}$ are at least C^1 on any *finite interval* of time $[0, t]$ (see, e.g., [12]). In this case, however, c is the solution of the diffusion equation and the magnitude of its gradient decays exponentially with time while c approaches its average, c_∞. As a result, the velocity field $\mathbf{v}$ also decays

exponentially in time. This is a sufficient condition for the trajectories $\mathbf{x}(t, \mathbf{x})$ to be C^1 on the *infinite* interval $t \in [0, +\infty[$. We define

$$\phi(\mathbf{x}_0) = \lim_{t \to +\infty} \mathbf{x}(t, \mathbf{x}_0).$$

The limit exists, is unique, and is a C^1 function of its argument $\mathbf{x}_0$. To check that this transformation is indeed a cartogram, recall that Liouville's theorem determines how area elements A change along trajectories:

$$\frac{\mathrm{d}}{\mathrm{d}t} \ln A \bigg|_{\mathbf{x}(t;\mathbf{x}_0),t} = \operatorname{div}(\mathbf{v}(\mathbf{x}, t)). \tag{4.1}$$

Direct computation shows that

$$\operatorname{div}(\mathbf{v}) = -\frac{\nu}{c}\Delta c + \frac{1}{\nu}\mathbf{v}^2.$$

Note that

$$\frac{\mathrm{d}}{\mathrm{d}t} \ln c = \frac{1}{c}\frac{\partial c}{\partial t} + \frac{\mathbf{v} \cdot \nabla c}{c} = -\operatorname{div}(\mathbf{v}).$$

As a result, Liouville's equation (4.1) simplifies to

$$A(t) = A(0)\, e^{-\int_0^t \frac{\mathrm{d}}{\mathrm{d}t} \ln c \, \mathrm{d}t} = A(0)\, \frac{c(\mathbf{x}_0, 0)}{c(\mathbf{x}, t)} = A(0)\, \frac{\rho(\mathbf{x}_0)}{c(\mathbf{x}, t)}.$$

For $t \to +\infty$, the density c becomes constant in space and we have

$$\det\left(\frac{\partial \phi}{\partial \mathbf{x}_0}(\mathbf{x}_0)\right) = \lim_{t \to +\infty} \frac{A(t)}{A(0)} = \frac{\rho(\mathbf{x}_0)}{c_\infty}.$$

Hence, the transformation $\phi(\mathbf{x}_0)$ is a cartogram since it changes area elements proportionally to $\rho(\mathbf{x}_0)$. Starting from an equal-area map (i.e., $A(0) = 1$), we can multiply $\phi(\mathbf{x}_0)$ by the constant c_∞ and the equality becomes

$$\det\left(\frac{\partial \phi}{\partial \mathbf{x}_0}(\mathbf{x}_0)\right) = \rho(\mathbf{x}_0).$$

By changing the name of the variable from $\mathbf{x}_0$ to $\mathbf{x}$, we obtain the desired form

$$\det\left(\frac{\partial \phi}{\partial \mathbf{x}}(\mathbf{x})\right) = \rho(\mathbf{x}).$$

4.2. Cartograms with moving boundaries. The conclusions reached for cartograms with constant boundaries do not translate immediately to cases where $\frac{\partial \rho}{\partial n} \neq 0$ on the boundary of the domain. In this case, we cannot apply the method described in the previous section, and theorems about existence and smoothness of the diffusion problem, as well as about the advection of the velocity field, are not applicable either. Gastner and Newman [9] suggest extending the density to a larger domain where Neumann boundary conditions are enforced. Given a function $\rho : \mathcal{D} \to \mathbb{R}_0^+$, one can select a larger domain $\mathcal{D}_0 \supset \mathcal{D}$ and pick an arbitrary function $\hat{\rho} : \mathcal{D}_0 \to \mathbb{R}_0^+$ such that $\hat{\rho}$ is identical to ρ in $\mathcal{D}$. Typically, $\mathcal{D}_0$ has an area of 4 or 9 times the initial domain $\mathcal{D}$. The goal is to design $\hat{\rho}$ in such a way that $\frac{\partial \hat{\rho}}{\partial n} = 0$ at the edges of the larger domain $\mathcal{D}_0$

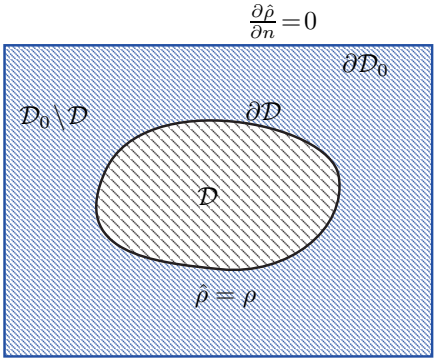

FIG. 3. *Proposed approach: when computing a cartogram for a domain $\mathcal{D}$ that has an arbitrary shape or for which the normal derivative of the density function ρ does not vanish at the boundary, a large rectangle $\mathcal{D}_0 \supset \mathcal{D}$ is selected. The density ρ is extended outside $\mathcal{D}$ by enforcing Neumann boundary conditions at the boundary of the large rectangle, requiring continuity of $\hat{\rho}$ at the edge with $\mathcal{D}$, and setting the Laplacian of $\hat{\rho}$ to a constant value outside $\mathcal{D}$. This defines a unique extension $\hat{\rho}$ which is continuous and has continuous derivatives almost everywhere.*

(see Figure 3). This permits the computation of the diffusion cartogram for the large domain $\mathcal{D}_0$ with fixed boundaries, followed by a restriction of the transformation to $\mathcal{D}$ to obtain the cartogram for the initial domain. This procedure is dependent on the choice of the embedding domain $\mathcal{D}_0$. Given $\mathcal{D}_0$, it also depends on how the extended density function $\hat{\rho}$ is constructed in $\mathcal{D}_0 \setminus \mathcal{D}$.

Gastner and Newman showed the importance of applying a "neutral buoyancy" condition, which keeps the total area under consideration constant. To construct $\hat{\rho}$, they first computed the average density in $\mathcal{D}$. In $\mathcal{D}_0 \setminus \mathcal{D}$, they filled $\hat{\rho}$ with a constant equal to the mean density in $\mathcal{D}$. They experimented with other choices of parameters, e.g., setting $\hat{\rho} = 0$ in $\mathcal{D}_0 \setminus \mathcal{D}$, but this resulted in inappropriate diffusion of density out of $\mathcal{D}$. The authors also experimented with different sizes for the domain $\mathcal{D}_0$ and observed only little visual difference, provided that $\mathcal{D}_0$ was sufficiently large.

From the point of view of our control design problem, the method above has an important flaw: $\hat{\rho}$, the initial condition for the diffusion problem, is not continuous at the boundary of $\mathcal{D}$. As a result, existence, uniqueness, and smoothness of the solution of the diffusion problem are not guaranteed. This is not necessarily a problem when producing only one cartogram. Our objective, however, is to produce continuous sequences of maps. Indeed, we will need the cartogram to vary smoothly when the density function is changed. For example, transferring Lyapunov functions from the cartogram space to the physical plane requires the existence of continuous derivatives.

As an alternative to Gastner and Newman's method, we propose the following variant. Given ρ in the domain of interest $\mathcal{D}$, we compute $\frac{\partial \rho}{\partial n}$ at the boundary of $\mathcal{D}$ and the total flux across $\partial \mathcal{D}$. We define the extended density $\hat{\rho}$ as follows:

- Inside $\mathcal{D}$, $\hat{\rho}(\mathbf{x}) = \rho(\mathbf{x})$.
- Outside $\mathcal{D}$, $\hat{\rho}$ is the solution of

$$\begin{cases} \Delta \hat{\rho} = \dfrac{-1}{\text{Area}(\mathcal{D}_0 \setminus \mathcal{D})} \displaystyle\int_{\mathcal{D}} \Delta \rho(\mathbf{x}) \, \mathrm{d}\mathbf{x} = \dfrac{-1}{\text{Area}(\mathcal{D}_0 \setminus \mathcal{D})} \oint_{\partial \mathcal{D}} \dfrac{\partial \rho}{\partial n} \, \mathrm{d}l, \\ \left. \dfrac{\partial \hat{\rho}}{\partial n} \right|_{\partial \mathcal{D}_0} = 0, \\ \hat{\rho}|_{\partial \mathcal{D}} = \rho|_{\partial \mathcal{D}}. \end{cases}$$

The equations above define $\hat{\rho}$ inside $\mathcal{D}_0 \setminus \mathcal{D}$ as the solution of a linear problem with inhomogeneous Neumann boundary conditions. The Laplacian of $\hat{\rho}$ is constant in $\mathcal{D}_0 \setminus \mathcal{D}$, and its value is set so it compensates exactly the flux through the inside hole $\mathcal{D}$. Indeed, Green's equality requires

$$\int_{\mathcal{D}_0} \Delta\hat{\rho} \, \mathrm{d}\mathbf{x} = \oint_{\partial\mathcal{D}_0} \frac{\partial\hat{\rho}}{\partial n} \, \mathrm{d}l = 0.$$

Since this problem is compatible, standard results in functional analysis [1, 6] guarantee that the solution is unique and belongs to the Sobolev space H_1, which contains the functions on $\mathcal{D}_0$ that are continuous everywhere and for which the derivatives are continuous almost everywhere.[1] This guarantees also that the resulting extended density, $\hat{\rho}$, can be used as the initial condition of the diffusion problem and provides a C^1 solution c. The resulting transformation $\phi(\mathbf{x})$ is unique and varies smoothly (i.e., in a C^1 fashion) when the input density ρ is changed.

The only possible inconvenience is the fact that the solution $\hat{\rho}$ may become negative in the embedding rectangle. In this case the solution $\phi(\mathbf{x})$ might not be continuous due to the factor $\nabla c/c$ in the equation giving the velocity field. Nevertheless, the diffusion equation shows that if the initial density $c(\mathbf{x}, 0) = \hat{\rho}(\mathbf{x})$ is positive, then the density at later times remains positive. In other words, the density remain positive for all of the points that initially had a positive density. While the cartogram might not be well defined for points which were initially located in regions where $\hat{\rho}$ was negative, it is always well defined for points of $\mathcal{D}$ where the initial density is the input function $\rho > 0$.

4.3. Numerical methods. Gastner and Newman showed how the diffusion problem on a rectangle can be efficiently solved using the Fourier transform of $c(\mathbf{x}, t)$. This transforms the problem into an ordinary differential equation where the variables are the Fourier coefficients [9]. The only difference between our procedure and that of Gastner and Newman is how the density ρ is extended from the domain of interest $\mathcal{D}$ to the larger square $\mathcal{D}_0$. The problem giving $\hat{\rho}$ is linear; hence we can mesh $D_0 \setminus D$ and use a Galerkin approximation of $\hat{\rho}$ (see [1, 6]). Figure 4 illustrates the computation of $\hat{\rho}$ in $\mathcal{D}_0 \setminus \mathcal{D}$ for the domain in Figure 2. To compute the cartogram in the right panel of Figure 2, the extended density $\hat{\rho}$ in Figure 4 was used to first derive a map of the large rectangle. This is a necessary step, as we do not expect the normal derivative of the population density (input) to vanish at the border of a country.

Note that the partial differential equation that we suggest to solve for determining the extended density $\hat{\rho}$ is linear. The time needed to solve the linear problem is therefore negligible with respect to the time that it would take to compute the nonlinear boundaries of the Voronoi cells for the non-Euclidean metric. Another advantage of the procedure used here is that there already exist many optimized linear algebra packages that can be used to compute directly the solution of the discretized differential equation.

5. Nonuniform coverage control.

5.1. Method. Cartograms can be used to extend any algorithm that minimizes the uniform coverage metric, based on the Euclidean distance, to an algorithm that minimizes a nonuniform coverage metric dependent on an arbitrary "weighted" distance d_ρ. Indeed, starting from a non-Euclidean distance d_ρ, a perfect cartogram

[1] By "almost everywhere" we mean that the derivatives are continuous everywhere, except, possibly, on sets of measure zero.

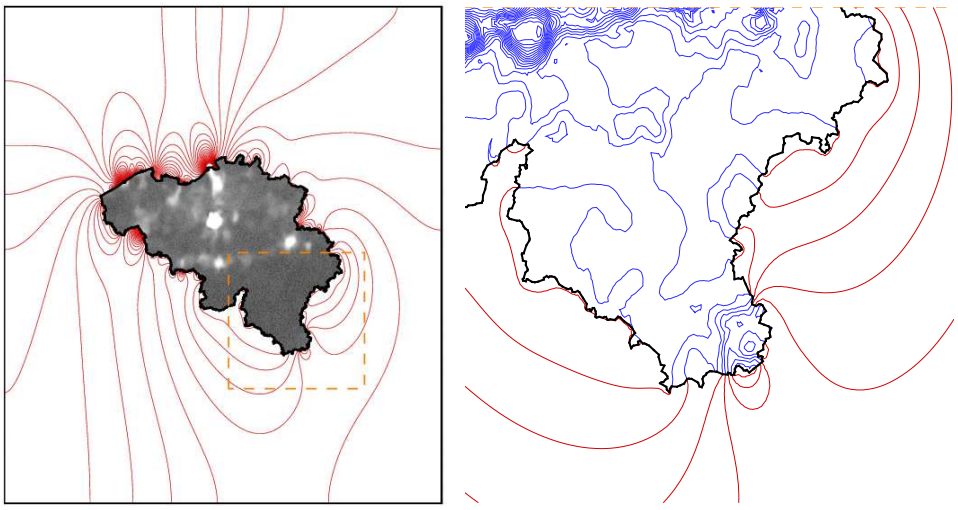

FIG. 4. *Continuous extension of the Belgian population density to a large rectangle with homogeneous Neumann boundary conditions. The extended density in the large rectangle is diffused to obtain the cartogram in the right panel of Figure* 2.

gives a transformation $\mathbf{y} = \phi(\mathbf{x})$ such that the distance function is Euclidean for $\mathbf{y}$. As a result, one can apply the uniform coverage algorithm to the $\mathbf{y}$ coordinates and prove convergence in the transformed space. In Theorem 5.1 (see section 5.3), we prove conditions under which convergence to the minimum of the uniform metric in the transformed space implies convergence to the minimum of the nonuniform metric in the original domain $\mathcal{D}$. The control law in the physical space for a system of agents with dynamics given by (2.1) can then be recovered from the chain rule as

$$\mathbf{u} = \dot{\mathbf{x}} = \left.\frac{\partial \phi^{-1}}{\partial \mathbf{y}}\right|_{\phi(\mathbf{x})} \dot{\mathbf{y}}.$$

5.2. Example. As an example, we let $\mathcal{D}$ be the unit square that was uniformly covered in Figure 1 using Cortés and Bullo's algorithm [4]. This time, however, we consider the multicenter coverage metric (2.2), where we replace the Euclidean distance d with a non-Euclidean distance d_ρ:

$$\Phi[d_\rho](\mathbf{x}_1, \mathbf{x}_2, \ldots, \mathbf{x}_n) = \max_{\mathbf{x}\in\mathcal{D}} \left\{ \min_{i=1\cdots n} d_\rho(\mathbf{x}, \mathbf{x}_i) \right\}. \tag{5.1}$$

For this example, we set the density function $\rho : \mathcal{D} \to \mathbb{R}_0^+$ to

$$\rho(x, y) = \frac{3}{40} + e^{-\frac{\left(x-\frac{3}{4}\right)^2+\left(y-\frac{1}{4}\right)^2}{\left(\frac{1}{10}\right)^2}},$$

which represents our nonuniform interest in the features contained inside the unit square, or the nonuniform roughness of the terrain. The density ρ is plotted in the left panel of Figure 5. In this example, the lower right quadrant of the unit square has a much higher density and must be covered more densely than the rest of the square. In the analogy with a group of animals, the peak at $\left(\frac{3}{4}, \frac{1}{4}\right)$ represents a region with larger food supply and the population concentrates more in the lower right quadrant.

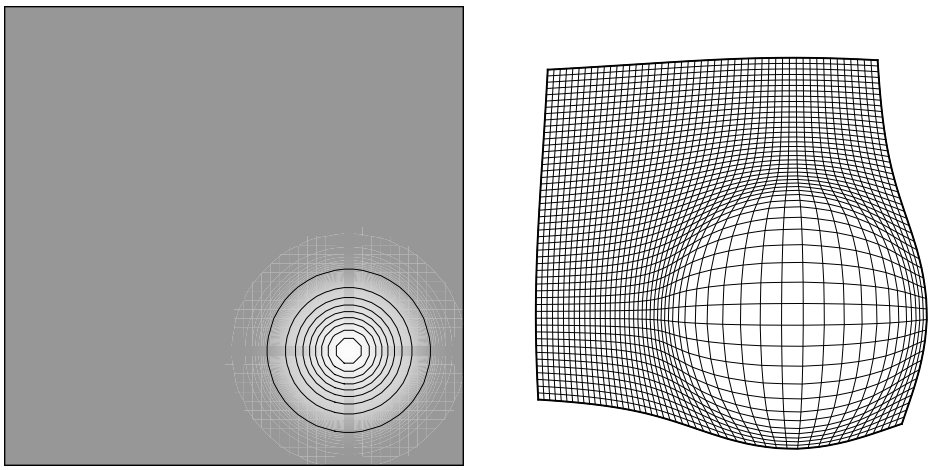

FIG. 5. *Cartogram of the unit square in preparation for nonuniform sampling.* Left panel: *Physical domain $\mathcal{D}$ with level sets of the density function* $\rho(x,y) = 0.075 + \exp\left(-\frac{(x-0.75)^2+(y-0.25)^2}{0.1^2}\right)$. Right panel: *Cartogram $\mathcal{D}'$ and image of a Cartesian mesh.*

In the analogy with a mine hunting array, the peak is a region where the robots move more slowly. To be able to respond anywhere in a minimum time, the vehicles must be closer to each other in the lower right quadrant.

To derive coverage control laws for $n = 4$ vehicles with dynamics given by (2.1), we first perform a cartogram of the area (see the right panel of Figure 5). The area near the peak of the Gaussian source is stretched by the transformation and represents about 30% of the mapped domain $\mathcal{D}'$, while it does not account for more than 10% of the physical domain $\mathcal{D}$.

To continue the example we apply the uniform coverage control law of [4] in the transformed plane $\mathcal{D}'$ which guarantees convergence to the optimal configuration in $\mathcal{D}'$. Figure 6 shows several snapshots of the motion of the particles in both $\mathcal{D}$ and $\mathcal{D}'$. Notice that the optimal configuration segments $\mathcal{D}'$ into four Voronoi cells of equal area, but, in the physical space, this corresponds to four (nonpolygonal) regions of unequal area; i.e., coverage is increased in the lower right quadrant.

Remark 1. Since the control is applied in a fictitious space, the norm of $\dot{\mathbf{y}}$ does not represent the actual speed of the vehicle. If unit speed control is desired (as in the simulation shown in Figure 6), then the velocity vector $\dot{\mathbf{y}}$ must be mapped back into the physical plane and normalized there.

Remark 2. The velocity in the cartogram is oriented along the segment between the vehicle and the circumcenter of its Voronoi cell. The preimage of this segment by the transformation is no longer a straight path. As a result, when the velocity vector is mapped back into physical coordinates by ϕ^{-1}, it is not necessarily oriented from the vehicle to the preimage of the circumcenter. Nevertheless, when the vehicle is infinitesimally close to the circumcenter, the two directions are aligned. At the equilibrium, the vehicles in the physical space are located exactly on the preimage of the circumcenter in the cartogram.

5.3. Proof of convergence. In this section, we prove that, given a feedback control law converging to a unique minimum of a cost function for the Euclidean metric, a perfect (or near perfect) cartogram provides a feedback control law that

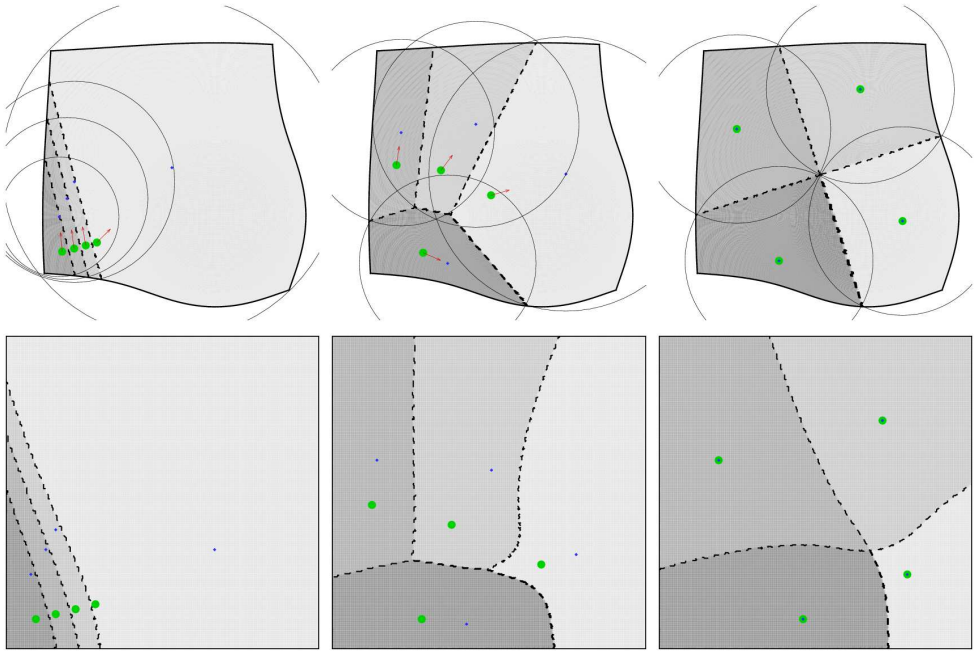

FIG. 6. *Convergence to static nonuniform coverage.* Thick dots: *Position of the four vehicles.* Shaded polygons: *Voronoi cell for each vehicle (computed in the cartogram space).* Large circles: *Circumcircle for each Voronoi cell of the cartogram.* Diamonds: *Centers of each circumcircle (i.e., circumcenters).* Arrows: *Instantaneous velocity of the vehicles (oriented along the segment joining the vehicle to the circumcenter of its Voronoi cell). The first row depicts the computation in the cartogram space. The second row gives the resulting positions of the vehicles in the physical space.*

converges to the unique minimum of the cost function for a non-Euclidean distance d_ρ defined by a density function $\rho > 0$.

Assume that a feedback control law has been designed and converges to the unique minimum of a cost function based on the Euclidean distance. We consider a nonuniform distance d_ρ and investigate how the control law for the Euclidean distance behaves in a near perfect cartogram of ρ. We show that, for C^1, strictly positive ρ, the non-Euclidean cost function has a unique minimum. Furthermore, the cartogram inverse-mapped feedback control converges toward this minimum.

THEOREM 5.1 (nonuniform coverage by cartograms). *Consider a C^1 cost function $(\Phi[d_\rho])(\mathbf{x}_i, \ldots, \mathbf{x}_n; \mathcal{D})$ that depends only on the distance $d_\rho(\mathbf{a}, \mathbf{b}) = \min_{c_\mathbf{a}^\mathbf{b}} \int_{c_\mathbf{a}^\mathbf{b}} \sqrt{\rho}\, \mathrm{d}l$ between n agent positions and points in the domain $\mathcal{D}$. We assume that Φ has a unique, nondegenerate minimum for the Euclidean distance $d_1(\mathbf{a}, \mathbf{b}) = \|\mathbf{a} - \mathbf{b}\|$. We also assume that there exists a feedback control law $\dot{\mathbf{x}}_i = \mathbf{v}_i(\mathbf{x}_1, \ldots, \mathbf{x}_n)$ that brings the vehicles to the minimum* for the Euclidean distance d_1.

Given a density function $\rho : \mathcal{D} \to \mathbb{R}_0^+$, consider a cartogram $\phi : \mathcal{D} \to \phi(\mathcal{D})$. We consider applying the control law for the Euclidean distance in the cartogram space; hence

$$\dot{\mathbf{y}}_i = \mathbf{v}_i(\mathbf{y}_1, \ldots, \mathbf{y}_n),$$

where $\mathbf{y}_i = \phi(\mathbf{x}_i)$. *The corresponding dynamics in the physical space* $\mathcal{D}$

$$\dot{\mathbf{x}}_i = \mathbf{u}_i = \left.\frac{\partial \phi^{-1}}{\partial \mathbf{y}}\right|_{\phi(\mathbf{x})} \dot{\mathbf{y}}_i$$

yield a convergent sequence. In the neighborhood of a perfect cartogram, we have the following:

1. *There is a unique minimum of* $(\Phi[d_\rho])(\mathbf{x}_i, \ldots, \mathbf{x}_n, \mathcal{D})$ *on* $\mathcal{D}$.
2. *The agents converge to an equilibrium that tends continuously to the unique minimum as* $\epsilon = \left\| \frac{\partial \phi}{\partial \mathbf{x}} - \sqrt{\rho}\, \mathbb{I} \right\| \to 0$.

Proof. By definition, a cartogram is a C^1 mapping

$$\phi : \mathcal{D} \to \phi(\mathcal{D}) : \mathbf{x} \mapsto \mathbf{y} = \phi(\mathbf{x}),$$

such that

$$\det\left(\frac{\partial \phi}{\partial \mathbf{x}}\right) = \rho.$$

This does not guarantee that the distance d_ρ between two points in the physical plane is equivalent to the Euclidean distance between the image of the two points in the cartogram. Nevertheless, the objective in computing the cartogram is to avoid unnecessary deformations, and, in the limit of a perfect cartogram, the equality of the distances is satisfied.

Consider a cartogram ϕ. The perfect cartogram is such that $\frac{\partial \phi}{\partial \mathbf{x}} = \sqrt{\rho}\, \mathbb{I}$, where $\mathbb{I}$ is the identity matrix. In section 6, we will show that the diffusion method described in this paper and in that of Gastner and Newman [9] provides a cartogram close to the ideal case for the examples that we studied. Developing the transformation about the perfect case, we get

$$\frac{\partial \phi}{\partial \mathbf{x}}(\mathbf{x}) = \sqrt{\rho}\, \mathbb{I} + \epsilon M(\mathbf{x}),$$

where $\|M\| = 1$ and $\epsilon = \left\| \frac{\partial \phi}{\partial \mathbf{x}} - \sqrt{\rho}\, \mathbb{I} \right\|$ is kept as small as possible to avoid distortions. For a perfect cartogram, we have $\epsilon \to 0$.

To investigate the relationship between distances in the physical space and in the cartogram, let us consider two points $\mathbf{x}_1$, $\mathbf{x}_2 \in \mathcal{D}$ and their images $\mathbf{y}_i = \phi(\mathbf{x}_i)$. We have

$$d_1(\mathbf{y}_1, \mathbf{y}_2) = \min_{\mathcal{C}_{\mathbf{y}_1}^{\mathbf{y}_2}} \int_{\mathcal{C}_{\mathbf{y}_1}^{\mathbf{y}_2}} \mathrm{d}l,$$

where $\mathcal{C}_{\mathbf{y}_1}^{\mathbf{y}_2}$ is an arbitrary path between points $\mathbf{y}_1$ and $\mathbf{y}_2$. Indeed, the Euclidean distance between two points $\mathbf{y}_1$ and $\mathbf{y}_2$ is the minimum length of the paths between the two points. Let us now apply the change of coordinates $\mathbf{y} = \phi(\mathbf{x})$. The infinitesimal arclength $\mathrm{d}l$ in the cartogram space becomes, in the physical space,

$$\sqrt{\mathbf{1}_l^\top \frac{\partial \phi}{\partial \mathbf{x}}^\top \frac{\partial \phi}{\partial \mathbf{x}} \mathbf{1}_l}\ \mathrm{d}l',$$

where $\mathbf{1}_l$ is the unit vector tangent to the path followed. As a result, we have

$$d_1(\mathbf{y}_1,\mathbf{y}_2) = \min_{\mathcal{C}_{\mathbf{y}_1}^{\mathbf{y}_2}} \int_{\mathcal{C}_{\mathbf{y}_1}^{\mathbf{y}_2}} \mathrm{d}l = \min_{\mathcal{C}_{\mathbf{x}_1}^{\mathbf{x}_2}} \int_{\mathcal{C}_{\mathbf{x}_1}^{\mathbf{x}_2}} \sqrt{\mathbf{1}_l^\top \frac{\partial\phi}{\partial\mathbf{x}}^\top \frac{\partial\phi}{\partial\mathbf{x}} \mathbf{1}_l}\ \mathrm{d}l' \tag{5.2}$$

$$= \min_{\mathcal{C}_{\mathbf{x}_1}^{\mathbf{x}_2}} \int_{\mathcal{C}_{\mathbf{x}_1}^{\mathbf{x}_2}} \sqrt{\rho + \epsilon\sqrt{\rho}\,\mathbf{1}_l^\top (M^\top + M)\mathbf{1}_l + \mathcal{O}(\epsilon^2)}\ \mathrm{d}l' \tag{5.3}$$

$$= \min_{\mathcal{C}_{\mathbf{x}_1}^{\mathbf{x}_2}} \int_{\mathcal{C}_{\mathbf{x}_1}^{\mathbf{x}_2}} \left[\sqrt{\rho} + \frac{\epsilon}{2\sqrt{\rho}}\ \mathbf{1}_l^\top (M^\top + M)\mathbf{1}_l + \mathcal{O}(\epsilon^2)\right]\ \mathrm{d}l' \tag{5.4}$$

$$= d_\rho(\mathbf{x}_1,\mathbf{x}_2) + \epsilon\, g(\mathbf{x}_1,\mathbf{x}_2) + \mathcal{O}(\epsilon^2), \tag{5.5}$$

where $\sqrt{\rho}\,\mathbf{1}_l^\top (M^\top + M)\mathbf{1}_l$ is continuous almost everywhere since ϕ is C^1 almost everywhere by definition. Notice that this also implies that $g(\mathbf{x}_1,\mathbf{x}_2) = \frac{\epsilon}{2\sqrt{\rho}} \int_{\mathcal{C}_{\mathbf{x}_1}^{\mathbf{x}_2}} \mathbf{1}_l^\top (M^\top + M)\mathbf{1}_l\ \mathrm{d}l$ is C^1 almost everywhere in its two arguments $\mathbf{x}_1$ and $\mathbf{x}_2$. As a result, the equation above states that the distance d_ρ between two points $\mathbf{x}_1$ and $\mathbf{x}_2$ in the physical space is equal to the Euclidean distance between the image of these two points in the cartogram $\phi(\mathbf{x}_1)$ and $\phi(\mathbf{x}_2)$, plus a correction $\epsilon\, g$ that vanishes continuously as $\epsilon \to 0$.

Since the cost function depends only on the distance between pairs of agents, between pairs of points in the domain $\mathcal{D}$, and between an agent and points of $\mathcal{D}$, we also have

$$\begin{aligned}(\Phi[d_\rho])\,(\mathbf{x}_1,\ldots,\mathbf{x}_n;\mathcal{D}) &= (\Phi[d_1])\,(\phi(\mathbf{x}_1),\ldots,\phi(\mathbf{x}_n),\phi(\mathcal{D})) \\ &\quad + \epsilon\, h(\mathbf{x}_1,\ldots,\mathbf{x}_n) + \mathcal{O}(\epsilon^2).\end{aligned} \tag{5.6}$$

Since g is a C^1 function of its arguments, h is also C^1 almost everywhere. In other words, when $\epsilon \to 0$, *the cost function for a configuration in physical space with a nonuniform metric tends in a C^1 fashion to the cost function for the mapped configuration in the cartogram but with the Euclidean distance.*

Let us consider the (unique) minimum of the cost function with the Euclidean distance:

$$\nabla_{\mathbf{y}}\,(\Phi[d_1])\,(\mathbf{y}_1^*,\ldots,\mathbf{y}_n^*;\phi(\mathcal{D})) = \mathbf{0}.$$

Recall that, by hypothesis, this minimum is unique and nondegenerate, i.e.,

$$\det\left(\left.\frac{\partial^2\Phi}{\partial\mathbf{y}^2}\right|_{\mathbf{y}^*}\right) \neq 0.$$

Furthermore, the hypotheses guarantee convergence of the control in the cartogram for the Euclidean distance; hence the agents converge to the configuration $\mathbf{y}^*$. Since ϕ and ϕ^{-1} are continuous, the vehicles in the physical plane converge to $\mathbf{x}_i^* = \phi^{-1}(\mathbf{y}_i^*)$.

For a perfect cartogram, using the chain rule, we find

$$\nabla_{\mathbf{x}}\,(\Phi[d_\rho])\,(\mathbf{x}_1,\ldots,\mathbf{x}_n;\mathcal{D}) = \underbrace{\left(\frac{\partial\phi}{\partial\mathbf{x}}\right)^{-1}}_{\det>0}\ \nabla_{\mathbf{y}}\,(\Phi[d_1])\,(\mathbf{y}_1,\ldots,\mathbf{y}_n;\phi(\mathcal{D}))\,.$$

Hence there is also one and only one minimum in the physical plane, and it is given by $\mathbf{x}_i^* = \phi^{-1}(\mathbf{y}_i^*)$. For a perfect cartogram, the vehicles converge exactly to the minimum of $\Phi[d_\rho]$.

For $\epsilon \neq 0$, the agents still reach the configuration $\mathbf{y}_i^*$ in the cartogram space. In the physical space, this still corresponds to the configuration $\mathbf{x}_i^* = \phi^{-1}(\mathbf{y}_i^*)$. In this case, however, $\mathbf{x}_i^*$ is not the minimum of $\Phi[d_\rho]$, and our goal is to show that the minimum of $\Phi[d_\rho]$ is still unique and that $\mathbf{x}_i^*$ is ϵ-close to this minimum. Starting from (5.6), we find

$$\nabla_{\mathbf{x}} \left(\Phi[d_\rho]\right)(\mathbf{x}_1, \ldots, \mathbf{x}_n; \mathcal{D}) = \left(\frac{\partial \phi}{\partial \mathbf{x}}\right)^{-1} \nabla_{\mathbf{y}} \left(\Phi[d_1]\right)(\mathbf{y}_1, \ldots, \mathbf{y}_n; \phi(\mathcal{D})) + \epsilon \nabla_{\mathbf{x}} h(\mathbf{x}_1, \ldots, \mathbf{x}_n) + \mathcal{O}(\epsilon^2),$$

where $\nabla_{\mathbf{x}} h$ is continuous almost everywhere. Hence, the (possibly multiply defined) minima of $\Phi[d_\rho]$ satisfy

$$\nabla_{\mathbf{y}} \left(\Phi[d_1]\right)(\mathbf{y}_1, \ldots, \mathbf{y}_n; \phi(\mathcal{D})) = -\epsilon \frac{\partial \phi}{\partial \mathbf{x}} \nabla_{\mathbf{x}} h(\mathbf{x}_1, \ldots, \mathbf{x}_n) + \mathcal{O}(\epsilon^2).$$

For $\epsilon = 0$, the unique solution is $\mathbf{y}^*$. For ϵ sufficiently small, our goal is to show that the minimum, seen as a function $\mathbf{y}^*(\epsilon)$, is single-valued and continuous in ϵ. This is precisely the scope of the implicit function theorem (see, e.g., [19]); this classical result states that, unless the derivative of the relation versus $\mathbf{y}$ is singular at $(\mathbf{y}, \epsilon) = (\mathbf{y}^*, 0)$, there exists such a C^1 curve of unique minima in a neighborhood of $\epsilon = 0$. Notice that the derivative of the implicit relationship at $\mathbf{y}^*$ and $\epsilon = 0$ is given by $\frac{\partial^2 \Phi}{\partial \mathbf{y}^2}\big|_{\mathbf{y}^*}$, which is nonsingular by assumption. As a result, the implicit function theorem guarantees that, for sufficiently small ϵ, there exists a unique minimum $\mathbf{y}(\epsilon)$ and, as $\epsilon \to 0$, this minimum converges in a C^1 fashion to $\mathbf{y}^*$.

Now that we know that the minimum is unique and varies smoothly with ϵ, we can find its location. Setting $\mathbf{y}(\epsilon) = \mathbf{y}^* + \epsilon \boldsymbol{\delta}$, we find

$$\mathbf{y}_i^\epsilon = \mathbf{y}_i^* - \epsilon \left(\frac{\partial^2 \Phi}{\partial \mathbf{y}^2}\right)^{-1}\Bigg|_{\mathbf{y}_i^*} \left.\frac{\partial \phi}{\partial \mathbf{x}}\right|_{\phi^{-1}(\mathbf{y}_i^*)} \nabla_{\mathbf{x}} h(\phi^{-1}(\mathbf{y}_i^*)) + \mathcal{O}(\epsilon^2).$$

This equation gives the coordinates (in the cartogram) of the minimum of $\Phi[d_\rho]$ (in physical space). The corresponding configuration in physical space is given by

$$\begin{aligned} \mathbf{x}_i^\epsilon &= \phi^{-1}(\mathbf{y}_i(\epsilon)) \\ &= \mathbf{x}_i^* - \epsilon \left(\frac{\partial \phi}{\partial \mathbf{x}}\right)^{-1}\Bigg|_{\mathbf{x}_i^*} \left(\frac{\partial^2 \Phi}{\partial \mathbf{y}^2}\right)^{-1}\Bigg|_{\phi^{-1}(\mathbf{y}_i^*)} \left.\frac{\partial \phi}{\partial \mathbf{x}}\right|_{\mathbf{x}_i^*} \nabla_{\mathbf{x}} h(\mathbf{x}_i^*) + \mathcal{O}(\epsilon^2). \end{aligned} \tag{5.7}$$

Notice that all of the matrices in the equation above are nonsingular. The minimum of $\Phi[d_\rho]$ is therefore also unique in the physical space and converges continuously to $\mathbf{x}^*$ as $\epsilon \to 0$.

Recall that $\mathbf{x}^*$ is the configuration to which the agents converge. $\mathbf{x}_i^\epsilon$ is the actual minimum of $\Phi[d_\rho]$. The equation above shows that, for small but nonzero ϵ, the optimum of the cost function with the nonuniform distance d_ρ is ϵ-close to the optimum of the cost function in the cartogram with the Euclidean metric. Furthermore, as $\epsilon \to 0$, the configuration of the agents converges continuously to the optimal configuration of the initial, non-Euclidean problem. ∎

6. Cartogram error. We have shown in the previous section that, given two points $\mathbf{x}_1$ and $\mathbf{x}_2$ in space and their images by the cartogram, $\phi(\mathbf{x}_1)$ and $\phi(\mathbf{x}_1)$, we have

$$d_1\big(\phi(\mathbf{x}_1),\phi(\mathbf{x}_2)\big) \leq d_\rho(\mathbf{x}_1,\mathbf{x}_2) + \frac{\epsilon}{2\sqrt{\rho}} \left\|M^\top + M\right\| + \mathcal{O}\left(\epsilon^2\right).$$

In the context of controlling vehicles in the cartogram space, convergence is guaranteed, provided that we can create a cartogram such that $d_1\big(\phi(\mathbf{x}_1),\phi(\mathbf{x}_2)\big)$ is sufficiently close to $d_\rho(\mathbf{x}_1,\mathbf{x}_2)$. Recall that $\epsilon = \left\|\sqrt{\rho}\,\mathbb{I} - \frac{\partial\phi}{\partial\mathbf{x}}\right\|$ and $\|M\| = 1$; hence,

$$\left|\frac{\epsilon}{2\sqrt{\rho}}\right| \left\|M^\top + M\right\| \leq \left\|\mathbb{I} - \frac{1}{\sqrt{\rho}}\frac{\partial\phi}{\partial\mathbf{x}}\right\| \doteq \eta$$

is the relevant unitless distortion factor for this problem.

Figure 7 shows the distribution of the deformation factor η for the test cartogram shown in Figure 5 as well as for the cartogram based on the Belgian population density. In both cases, the maximum deformation factor η is below 0.4. Figure 7 shows also that the deformation is below 0.1 in a very high fraction of the total area. The distortion factor η grows above 0.1 only in small bands separating regions of very different densities. For example, there is a narrow annulus of high distortion around the density peak in the lower right corner of the left panel of Figure 7.

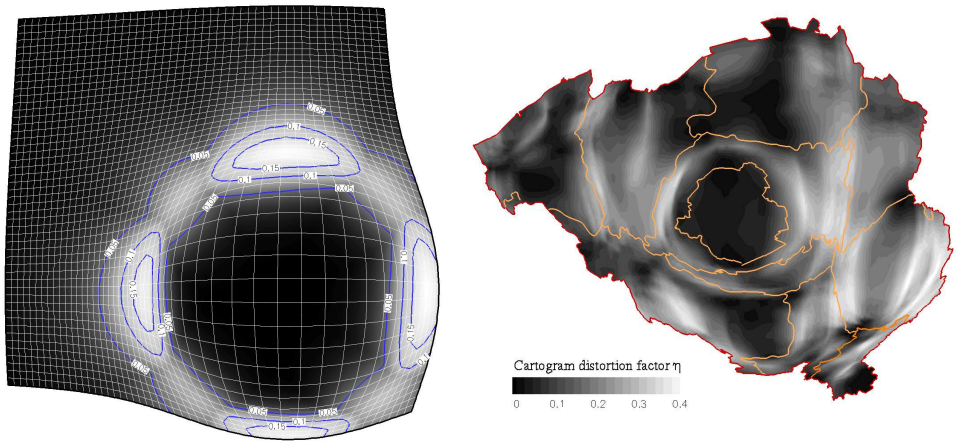

FIG. 7. *Level sets of the distortion factor* $\eta = \left\|I - \frac{1}{\rho}\frac{\partial\phi}{\partial\mathbf{x}}\right\|$ *for the cartograms constructed in Figure* 5 *(left panel) and in Figure* 2 *(right panel).*

It is worth noting that (5.7) indicates that we can always multiply the cost function Φ by an arbitrary large number to reduce the influence of the distortion factor. In the case of the example of section 5.2, the error can be estimated as follows: we have $\rho < 1.075$ and Figure 7 shows that, at the equilibrium positions, we have $\eta < 0.1$. As a result we have $\epsilon = \left\|\sqrt{\rho}I - \frac{\partial\phi}{\partial\mathbf{x}}\right\| = \sqrt{\rho}\,\eta < 0.11$. The error is given by $\frac{\epsilon}{2\sqrt{\rho}} = \frac{\eta}{2} < 0.05$, which is to be compared to the unit side of the square domain.

7. Space-time optimal coverage. In most problems, the metric does not remain constant in time. Indeed, when the density ρ is a physical quantity, such as the refractive index, it changes according to the fluctuations in the environment (e.g.,

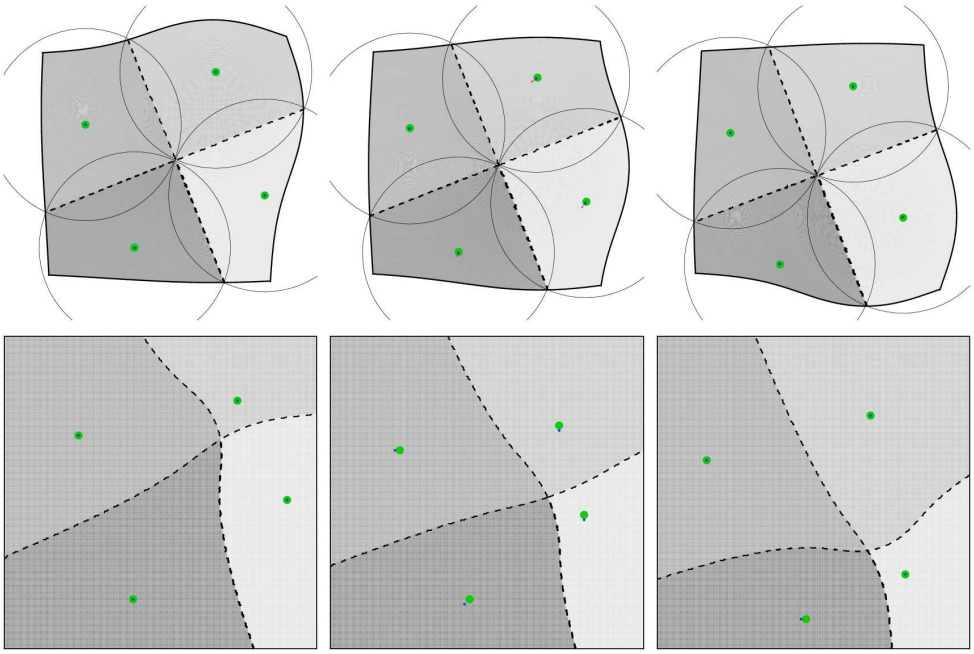

FIG. 8. *Convergence to nonuniform coverage with time-varying density.* Thick dots: *Position of the four vehicles.* Shaded polygons: *Voronoi cell for each vehicle (computed in the cartogram space).* Large circles: *Circumcircles for each Voronoi cell of the cartogram.* Diamonds: *Centers of each circumcircle (i.e., circumcenters).* Arrows: *Instantaneous velocity of the vehicles (oriented along the segment joining the vehicle to the circumcenter of its Voronoi cell). The first row depicts the computation in the cartogram space. The second row gives the resulting positions of the vehicles in the physical space. From left to right, the snapshots are taken when the peak of density is in the upper right corner, at* $y = \frac{1}{2}$*, and in the lower right corner.*

sources, sinks, diffusion, advection). When the nonuniform density represents information or food, its variations over time are even more subtle: the agents cover the domain and concentrate in regions of high density, but, at the same time, they deplete food or gather information and, in doing so, erode the very density peaks that attracted them. One such example is the objective analysis (OA) information map in [15].

The method developed in this paper is well suited for such time-varying metrics. Indeed, the numerical method presented in section 4 is aimed at producing cartograms that depend smoothly on the density function ρ. In other words, for a density function $\rho(\mathbf{x}, t)$ that is C^1 in time, we find a family of cartograms $\phi_t : \mathcal{D} \to \mathcal{D}'_t$ where both the transformation ϕ_t and the transformed space $\mathcal{D}'_t$ change with time in a C^1 fashion.

As an example, we modify the density function ρ from section 5.1 as follows:

$$\rho(x, y) = \frac{3}{40} + e^{-\frac{\left(x-\frac{3}{4}\right)^2+\left(y-\frac{1}{2}+\frac{1}{4}\cos\left(\frac{t}{2\pi}\right)\right)^2}{\frac{1}{10}^2}}.$$

In other words, the peak of the distribution ρ now moves periodically along the vertical axis $x = \frac{3}{4}$. Figure 8 shows the result of this simulation for four agents. For the snapshots on the left, the peak of density is at its maximum position in the upper right quadrant. For the snapshots on the right, the peak is at the minimum in the lower right quadrant. The middle panels correspond to an intermediate position.

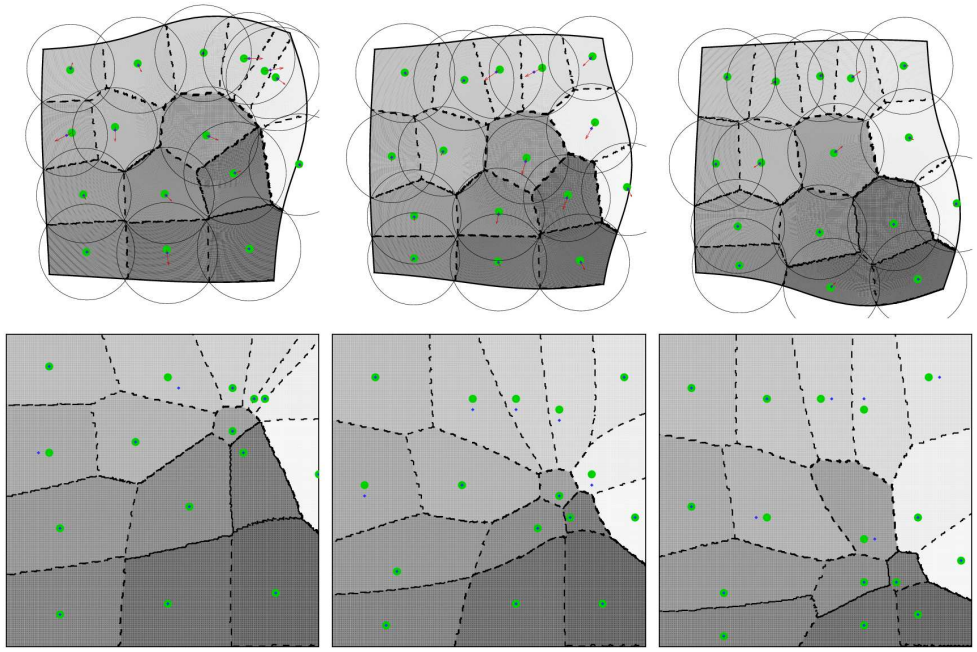

FIG. 9. *Array of* 10 *agents covering the square with nonuniform, time-varying density. On the left, the peak of density is in the upper right quadrant; on the right, the peak is in the lower right quadrant. The middle panel is an intermediate snapshot.*

Notice that, despite the fact that the optimal configuration changes a lot in physical space, the cartograms are similar to each other. This highlights one of the advantages of the method: the complexity of the nonuniform and time-varying density is absorbed in the cartogram transformation. In the cartogram plane, a simpler, uniform coverage algorithm is applied.

In Figure 9, the same simulation is performed for 10 vehicles, and it shows how the agents organize and move to follow the peak in the density ρ.

For autonomous, nonuniform metrics, we proved uniqueness of the optimal configuration and convergence to this position. The algorithm applies well to the case of time-varying metrics. If the density function changes slowly enough (in comparison to agent speed) and, at any time t, the distortion $\eta(t) = \left\| \mathbb{I} - \frac{1}{\sqrt{\rho(t)}} \frac{\partial \phi}{\partial \mathbf{x}}(t) \right\|$ is sufficiently small, then convergence can be inferred by our theorem. The requirement that $\rho(t)$ does not change too fast guarantees that the cartogram does not change too fast, and, hence, the boundary $\phi(\mathcal{D})$ does not change too fast with respect to vehicle speed. As a result, the motion of the cartogram boundary (slow dynamics) and the motion of the vehicles (fast dynamics) are almost decoupled, and we infer convergence from the fact that vehicles are converging to the equilibrium on timescales much shorter than the timescale at which $\phi(\mathcal{D})$ changes.

For a fast changing metric, there are two possible obstacles that can limit the use of the method that we proposed. First, a fast changing metric might make the cartogram boundary move too fast for the vehicle to converge to any configuration. Second, if the vehicles converge, then the configuration reached might differ significantly from the minimum of the metric.

8. Conclusions. In this paper, we investigated the use of cartograms to achieve time-varying, nonuniform coverage of a spatial domain by a group of agents. The method proposed relies on the existence of a stable algorithm that achieves uniform coverage (e.g., for the Euclidean metric). The control law is extended to nonuniform coverage (based on a non-Euclidean distance induced by a density function) by the use of density-equalizing maps.

The advantage of the method presented is its universality: it permits generalizing many existing uniform coverage algorithms to nonuniform metrics. It also provides a simple and fast control law. For example, computing Voronoi cells with a nonuniform metric is, in comparison, a very time-consuming operation.

The control law presented in this paper is not distributed. In particular, the diffusion equation uses information from all agents and is computed on a central computer. However, a distributed version of the proposed approach may be possible, provided that each agent computes its own local diffusion equation. In this case information passed from neighbors would be used to determine boundary conditions.

Another limitation of the method presented in this paper is the fact that it applies only to simple vehicle dynamics (first-order control). Although it is possible to find heuristic adaptations to nonholonomic constraints, uniqueness of the optimal configuration and convergence are not guaranteed by the results presented in this paper. The major difficulty is that nonholonomic constraints, unlike distances and cost functions, are not preserved by the cartogram mapping.

An inspiration for this work comes from a desire to understand how animal groups organize themselves to exploit a time-varying nonuniform food supply. Other applications are numerous, as teams of unmanned robots are often destined to tasks for which they need to mimic foraging animals. In [15], underwater vehicles patrol the ocean to collect scientific data. Information for these agents is analogous to food: the vehicles "consume" information by going to unsampled areas and lowering the uncertainty. After a region has been visited, uncertainty grows in time, analogous to the growing "food source."

OA provides a framework to study quantitatively these systems by estimating the residual error (or negative information) for an array of agents. It has been used successfully to optimize the design of static and moving arrays [3, 15]. The method presented in this paper is designed to match the OA model. Indeed, the residual error corresponds to the input density ρ. Adequate data sampling is a key ingredient in providing accurate ocean models. Recent developments in ocean modeling provide detailed error maps [16] that can be equally used as the input density of our method. Our objective is to optimize the motion of sampling agents in such a way that the residual error in the models assimilating these data is minimum. From this point of view, the cartograms represent an abstraction layer between a complex objective (minimize error in large scale ocean models) and the control algorithm itself.

Acknowledgments. The authors are grateful to Russ Davis (Scripps Institution of Oceanography), Pierre Lermusiaux (MIT), and David Fratantoni (Woods Hole Oceanographic Institution) for enlightening discussions about underwater glider control and ocean sampling. The Fourier transforms needed to solve the diffusion equation on rectangles were performed using FFTW, the "fastest Fourier transform in the West" [8]. Finite-element approximations of the linear partial differential equation problems defining the extended density function between the domain of interest and a larger embedding rectangle were obtained using libsparse, a C++ wrapper to the University of Florida's UMFPack (see documentation of the OMA package or [13, 14]).

REFERENCES

[1] J.-P. Aubin, *Applied Functional Analysis*, Pure Appl. Math. (N.Y.), Wiley-Interscience, New York, 2000.

[2] C. Bernstein, A. Kacelnik, and J. R. Krebs, *Individual decisions and the distribution of predators in a patchy environment*, J. Animal Ecology, 57 (1988), pp. 1007–1026.

[3] F. P. Bretherton, R. E. Davis, and C. B. Fandry, *A technique for objective analysis and design of oceanographic experiments applied to MODE-73*, Deep-Sea Res., 23 (1976), pp. 559–582.

[4] J. Cortés and F. Bullo, *Coordination and geometric optimization via distributed dynamical systems*, SIAM J. Control Optim., 44 (2005), pp. 1543–1574.

[5] J. Cortés, S. Martínez, T. Karatas, and F. Bullo, *Coverage control for mobile sensing networks*, IEEE Trans. Robotics and Automation, 20 (2004), pp. 243–255.

[6] B. Daya Reddy, *Introductory Functional Analysis*, Springer-Verlag, New York, 1997.

[7] S. D. Fretwell and H. L. Lucas, Jr., *On territorial behavior and other factors influencing habitat distribution in birds*, Acta Biotheoretica, 19 (1970), pp. 16–36.

[8] M. Frigo and S. G. Johnson, *The design and implementation of FFTW3*, Proc. IEEE, 93 (2005), pp. 216–231.

[9] M. T. Gastner and E. J. Newman, *Diffusion-based method for producing density-equalizing maps*, Proc. Natl. Acad. Sci. USA, 101 (2004), pp. 7499–7504.

[10] M. T. Gastner and E. J. Newman, *Optimal design of spatial distribution networks*, Phys. Rev. E (3), 74 (2006), 016117.

[11] M. T. Gastner, C. R. Shalizi, and E. J. Newman, *Maps and cartograms of the 2004 US presidential election results*, Adv. Complex Syst., 8 (2005), pp. 117–123.

[12] M. W. Hirsch and S. Smale, *Differential Equations, Dynamical Systems and Linear Algebra*, Academic Press, New York, 1974.

[13] D. M. Kaplan and F. Lekien, *Spatial interpolation and filtering of surface current data based on open-boundary modal analysis*, J. Geophys. Res. [Oceans], 112 (2007), C12007.

[14] F. Lekien, C. Coulliette, R. Bank, and J. Marsden, *Open-boundary modal analysis: Interpolation, extrapolation, and filtering*, J. Geophys. Res. [Oceans], 109 (2004), C12004.

[15] N. E. Leonard, D. Paley, F. Lekien, R. Sepulchre, D. M. Fratantoni, and R. Davis, *Collective motion, sensor networks and ocean sampling*, Proc. IEEE, 95 (2007), pp. 48–74.

[16] P. F. J. Lermusiaux, *Uncertainty estimation and prediction for interdisciplinary ocean dynamics*, J. Comput. Phys., 217 (2006), pp. 176–199.

[17] W. Li and C. G. Cassandras, *Distributed cooperative coverage control of sensor networks*, in Proceedings of the 44th IEEE Conference on Decision and Control, 2005, pp. 2542–2547.

[18] S. Poduri and G. S. Sukhatme, *Constrained coverage for mobile sensor networks*, in Proceedings of the IEEE International Conference on Robotics and Automation, 2004, pp. 165–172.

[19] W. Rudin, *Principles of Mathematical Analysis*, McGraw–Hill, New York, 1976.

[20] D. W. Stephens and J. R. Krebs, *Foraging Theory*, Princeton University Press, Princeton, NJ, 1986.